Int. J. Electrochem. Sci., 15 **(2020)** 265 – 279, doi: 10.20964/2020.01.02

International Journal of ELECTROCHEMICAL SCIENCE
www.electrochemsci.org

Synthesis of Biomass-Based Porous Carbon Nanofibre/Polyaniline Composites for Supercapacitor Electrode Materials

Debin Kong, Caiyun Qin, Lin Cao, Zeming Fang, Fenglin Lai, Zhidan Lin[*]*, Peng Zhang*[*]*, Wei Li, Huaijun Lin*

Institute of Advanced Wear & Corrosion Resistant and Functional Materials, Jinan University, Guangzhou, 510632, P.R. China.
[*]E-mail: linzd@jnu.edu.cn, tzhangpeng@jnu.edu.cn

Received: 19 July 2019 / *Accepted:* 3 September 2019 / *Published:* 30 November 2019

Carbonized bacterial cellulose (CBC) nanofibre surfaces coated with polyaniline(PANI) were successfully designed and prepared via in-situ polymerization with different dopant acids (i.e., H_3PO_4 and TsOH). By combining the high-specific-area CBC nanofibres and conductive PANI, the CBC/PANI composite electrode exhibited greatly improved capacitive performance. The specific capacitance of CBC/PANI-T-0.5 reached 324.8 F/g at 1 A/g. Moreover, the as-assembled CBC/PANI-T-0.5//N, P-CBC asymmetric supercapacitor showed good capacitance, great rate performance and good long-term cycling performance, distinctly demonstrating that the CBC/PANI-T composite is a promising electrode material for supercapacitor devices.

Keywords: Carbon nanofibres; Polyaniline; Supercapacitor; Composite materials; Electrode

1. INTRODUCTION

An electrochemical supercapacitor is a device that can quickly charge and discharge stored energy between a battery (having a high energy density) and a conventional capacitor (having a high output power)[1,2]. Supercapacitors have broad application prospects in the fields of national defence, aerospace and portable communication equipment. According to different working mechanisms, supercapacitors are divided into two classes[3,4]: electrochemical double-layer capacitors and pseudocapacitors. In an electric double-layer capacitor electric charges are stored by an electric double layer formed by ion adsorption-desorption on the surface of an electrode material and an electrolyte. Currently, graphene[5-7], carbon nanotubes[8-10] and activated carbon[11,12] are the most common carbon electrode materials with high specific surface areas. Pseudocapacitors mainly use redox reactions on the surface or in the bulk of the electrode materials, including conductive polymer[13-15]and

transition metal oxides[16-19], to store energy.

Bacterial cellulose (BC) is a green, environmentally friendly and renewable biomass material with abundant sources, low preparation costs and a simple preparation process[20]. From the point of view of composition, it is a pure cellulose material, that does not contain pectin, lignin, hemicellulose or other plant components, so it does not need pretreatment or impurity removal. From the microstructure point of view, BC is composed of cellulose nanofibres with a diameter of 20~100 nm. It has a unique and complex three-dimensional porous network. In addition, BC also exhibits high hydrophilicity, excellent biocompatibility and non-toxicity. More importantly, the carbonized products prepared by high temperature pyrolysis of BC under the protection of an inert atmosphere can maintain an intact fibre structure and three-dimensional porous network of BC[21,22]. This porous structure is beneficial to accelerate the entry of the electrolyte and the migration and diffusion of ions, so BC-based carbon materials have better electrochemical properties in the field of supercapacitors, as found in recent studies. However, carbonated bacterial cellulose is a double-layer capacitor material, which is limited in its practical application in supercapacitors because of its low specific capacitance and energy density.

Conductive polymers with a high specific capacitance,low cost, simple preparation and excellent chemical stability have received great attention[23-25]. The conductive polymers store energy by a redox reaction. When oxidation occurs, the doped ions migrate into the conductive polymer skeleton; when the reduction process occurs, the ions leave the conductive polymer skeleton and return to the electrolyte. The redox reaction occurs not only on the surface of the polymer but also in the interior. Although conductive polymers have many advantages, the doping/de-doping ions of the redox process may lead to the expansion and contraction of the polymer skeleton, causing deterioration of the polymer, thereby seriously affecting the cycle stability of the supercapacitor electrode materials. Carbon nanomaterials can support the conductive polymer, limit its expansion and contraction, and fully utilize the pseudocapacitance of the conductive polymers. The combination of conductive polymer and carbon nanomaterials can not only improve the conductivity, but also combine the advantages of the two materials, which can enhance the electrochemical performance of the composite due to the synergistic effect of the conductive polymer and carbon nanomaterials. Research on carbon nanotubes and conductive polyaniline composite supercapacitors has been reported in many studies[26-28], but studies on the preparation of polyaniline and carbon nanofibre composite supercapacitors are still relatively rare.

In this study, CBC/PANI materials were successfully prepared by in-situ polymerization with different aqueous dopant acids (i.e., H_3PO_4 and TsOH), and named CBC/PANI-P and CBC/PANI-T composite, respectively. The CBC/PANI-T-0.5 electrode, exhibited a higt capacitance (324.8 F/g at 1A/g) in H_2SO_4. In addition, an asymmetric supercapacitor using a positive electrode based on this CBC/PANI-T-0.5 material exhibited good capacitance, a great rate performance and good long-term cycling performance.

2. EXPERIMENTAL

2.1 Materials

Bacterial cellulose (BC, 320 × 240 × 3 mm^3) was purchased from Hainan Yide Food Co. Ltd.,

China. Aniline (ANI), ammonium persulfate [$(NH_4)_2S_2O_8$, APS], and phosphoric acid (H_3PO_4) were all purchased from Tianjin Damao Chemical Reagent Company, China, and were of analytical grade. P-toluene sulfonic acid (p-$CH_3C_6H_4SO_3H$, TsOH) was purchased from Tianjin Baishi Chemical Industry Co. Ltd., China., and was of analytical grade. All chemicals in this work were used directly without further purification.

2.2 Preparation of CBC Nanofibre

CBC nanofibres were prepared by the method described in our previous study[29]. In brief, BC was washed to neutral with deionized water, pre-frozen with liquid nitrogen (–196℃) for 30 min, and then freeze-dried at–50℃ for 24 h to obtain BC freeze-dried samples. These samples were placed in a tubular sintering furnace filled with N_2 gas for pyrolysis. The pyrolysis heating procedure was as follows: it is first heated to 240℃ at a heating rate of 5°C/min and kept for 1 h; then the sample was heated from 240–400°C,at a slower heating rate of 0. 5°C/min. Finally, a heating rate of 5°C/min was used to reach 800°C and this temperature was maintained for 2 h. The carbonized bacterial cellulose was named CBC-800.

2.3 Preparation of CBC/PANI Composite

Polyaniline was synthesized through the oxidative polymerization method. In a typical synthesis, 30 mg CBC nanofibre powder was added to 30 mL TsOH aqueous solution (0.1 M) and dispersed by ultrasonication for 30 min. Then 150 μL aniline monomer was added into the above solution and stirred for 1 h to generate a homogeneous suspension. The next step wes oxidative polymerization of aniline monomers for which 10 mL TsOH aqueous solution (0.1 M) containing 375 mg APS was added dropwise at room temperature to synthesize polyaniline (PANI). The reaction was continued for 4 hours. After the reaction was completed, the solution was filtered to obtain the product, which was washed repeatedly with ethanol and deionized water. Then, the samples were dried at 60°C for 24 h to obtain a composite compositie of polyaniline covered in carbonize bacterial cellulose, which was named CBC/PANI-T-0.1 composite. Moreover, the dopant acid TsOH (0.1 M) was changed to H_3PO_4 (0.1 M) to acquire the corresponding composite, which was denoted as the CBC/PANI-P-0.1 composite. The rough synthesis process of the CBC/PANI composites is shown in Figure 1a.

In addition, the doping concentration of TsOH in CBC/PANI-T was adjusted in the experiment. Here, CBC/PANI-T-0.1, CBC/PANI-T-0.5, and CBC/PANI-T-1.0 were prepared with 0.1 M, 0.5 M and 1.0 M aqueous TsOH aqueou solution, respectively.

2.4 Materials Characterization

The morphology of CBC/PANI composites was investigated by field emission scanning electron microscopy (FESEM)(Ultra55, ZEISS). The phase structures of the samples were tested by an X-ray diffractometer (XRD)(Rigaku Ultima IV) with a Cu Kα radiation source(λ = 0.1542 nm) at 40 kV and 40 mA. The phase composition of the samples was analysed with Fourier transform infrared (FT-IR)

spectrometry (Vertex 70, Bruker) and thermogravimetric analysis (TGA)(TGA/DSC 3+, Mettler Toledo).

2.5 Electrochemical Measurement with a Three-Electrode System

All electrochemical performance tests were conducted on an electrochemistry workstation(Princeton P4000, USA) .Using a three-electrode cell with 6 M KOH electrolyte for testing, a Ag/AgCl electrode was used as the reference electrode and a Pt electrode was used as the counter electrode. The active material, acetylene black, and 5 wt% polytetrafluoroethylene were mixed at a mass ratio of 8:1:1 as the working electrode . Then,the mixture was coated on foamed nickel(1 cm × 1 cm) and dried overnight at 100 °C, and pressure applied to form a sheet. The amount of active material of the pre-tested electrodes was controlled at 1 ~ 2 mg.Cyclic voltammograms (CV) was measured at different scan rates over a range from -0.2 to 0.8 V. Galvanostatic charge–discharge (GCD) behaviour was investigated in a voltage window of 0 ~ 0.8 V, and the current density was set to 1~5 A/g. Electrochemical impedance spectroscopy (EIS) was performed in a frequency range of 10 mHz to 100 kHz and at applied an AC signal of 5 mV.

3. RESULTS AND DISCUSSION

After pyrolysis, CBCs nanofibres can maintain their original three-dimensional network structure. In Figure 1b, the CBC-800 sample is composed of numerous intertwined nanofibres with a relatively smooth, and the diameter of the fibres is approximately 20~50 nm.

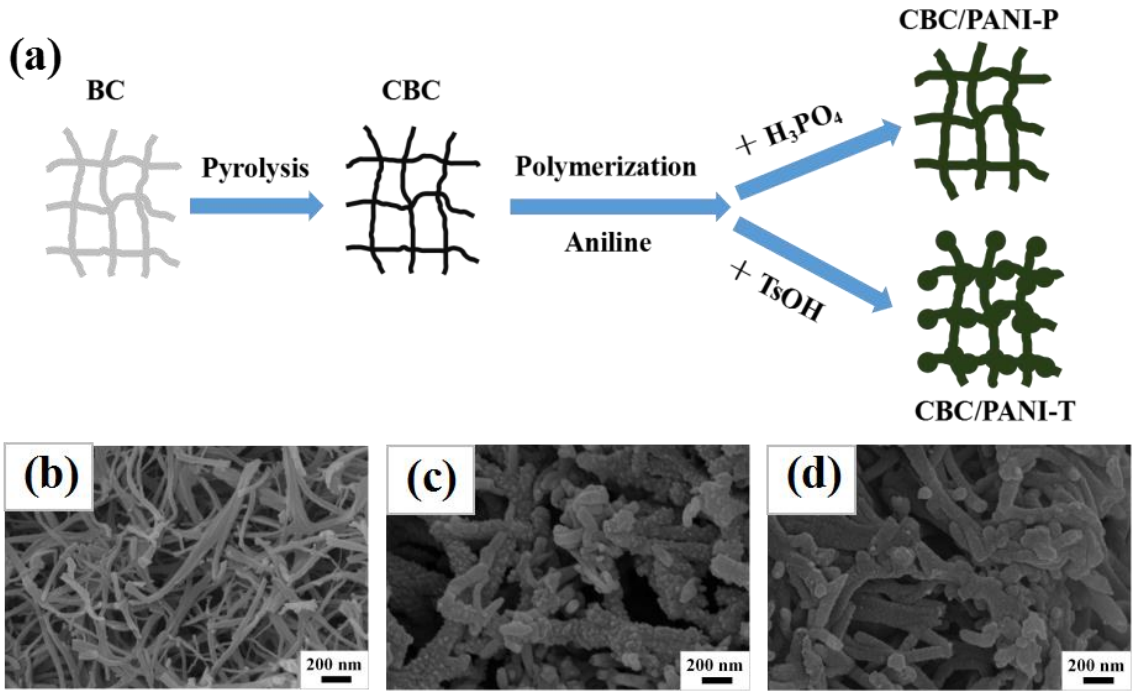

Figure 1. (a) Schematic diagram illustration of the synthesis of CBC/PANI composites; FESEM images of (b); CBC-800 nanofibres; (c) CBC/PANI-T-0.1 composite and (d) CBC/PANI-P-0.1 composite.

This 3D network structure is an ideal template that can be used for the growth of polyaniline. CBC/PANI-T-0.1 and CBC/PANI-P-0.1 composites consisting of nanosized fibres are shown in Figure 1c and d. The surface of the fibres became rough, and the diameter increased relative to that of the CBC-800 sample. It is clearly observed that the PANI nanoparticles adhere to the surface of the carbon nanofibres, which indicates that PANI has been successfully prepared and coated on the CBC nanofibres. From the SEM diagrams, it can also be found that the average fibre diameter of the CBC/PANI-T-0.1 composite (120 nm) is significantly larger than that of CBC/PANI-P-0.1 (70 nm). In the process of polymerization, the concentration of doped acid (TsOH and H_3PO_4) is the same (0.1 M); however, the ionic radius of the organic acid anion ($CH_3C_6H_4SO_3^-$) is much larger than that of the inorganic acid anion (such as PO_4^{3-}, $H_2PO_4^-$ and HPO_4^{2-} ions)[30]. Polyaniline with a rigid molecular chain structure is affected by steric hindrance. A larger ionic radius and a stronger steric effect can decrease the rate of polymerization and provide sufficient space to complete the nucleation and molecular chain growth of PANI.

The chemical bond structures and phases of different specimens were characterized via FT-IR and XRD techniques. As in the previous literature[29], the CBC-800 sample possesses two broad diffraction peaks at 2θ = 24.7° and 43.5°, which correspond to the characteristic (002) and (101) peaks of carbon, confirming that the CBC-800 sample is an amorphous carbon material with a low degree of graphitization (Figure 2a). Importantly, two relatively strong diffraction peaks observed at 2θ = 20.1° and 25° for the CBC/PANI-T-0.1 and CBC/PANI-P-0.1 composites (Figure 2a) can be ascribed to the (020) and (200) crystal planes of PANI[31], respectively, indicating that the pre-synthesized PANI molecular chain is partially crystallized. In addition, a broad peak at 43.5° was observed in the XRD patterns of the CBC/PANI-T-0.1 and CBC/PANI-P-0.1 composites (Figure 2a), which proves that PANI has successfully grown on the surface of the CBC nanofibres.

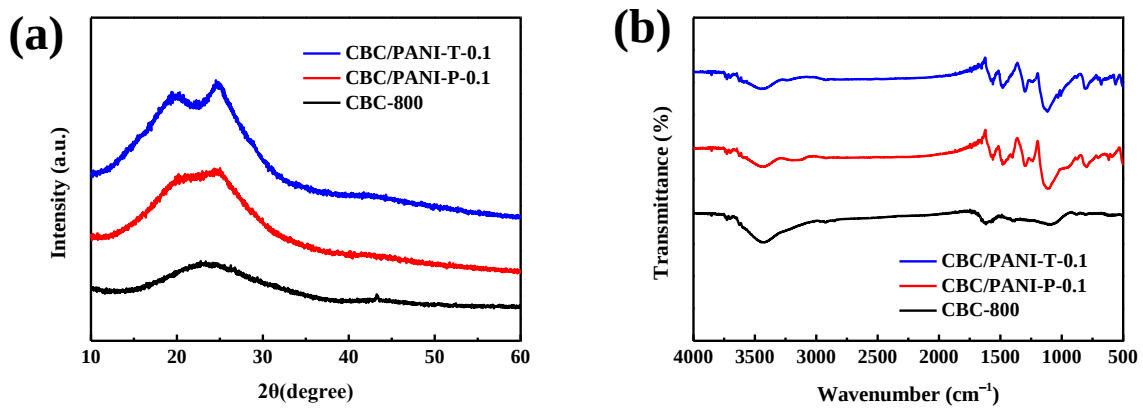

Figure 2. (a) XRD patterns and (b) FT-IR spectra of CBC-800, CBC/PANI-T-0.1 and CBC/PANI-P-0.1 composites.

The IR spectra of CBC-800, CBC/PANI-T-0.1 and CBC/PANI-P-0.1 composites are shown in Figure 2b. Sample CBC-800 shows four kinds of absorption peaks: the bands located at 3423 cm^{-1}, 1617 cm^{-1}, 1401 $cm^{-1,}$ and 1091 cm^{-1} are attributed to aromatic ring C-H stretching vibrations, benzene ring C=C stretching, C=O stretching and C-O stretching, respectively. Compared with the spectrum of CBC-800, the spectra of CBC/PANI-T-0.1 and CBC/PANI-P-0.1 composites show several characteristic

peaks of PANI[32]. The peaks at 1560 cm^{-1} and 1298 cm^{-1} are due to the stretching vibration of quinonoidal C=C and C-N bonds. The bands at 1467 cm^{-1} and 1116 cm^{-1} correspond to benzenoidal C=C and C=N stretching, respectively. The vibration at 827 cm^{-1} is attributable to the bending/benzene ring deformation of the functional group C-H. The IR results also verified that PANI had been successfully synthesized on the surface of CBC, which is consistent with the results of the XRD spectra. To compare the coating amount of PANI in CBC/PANI composites synthesized in various doped acids, the TGA curves of CBC-800, CBC/PANI-T-0.1 and CBC/PANI-P-0.1 samples are shown in Figure 3.

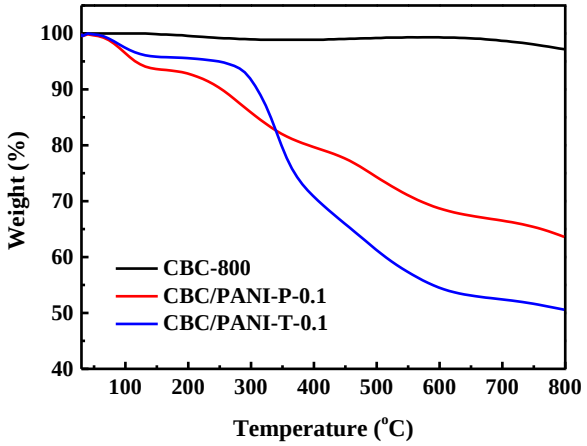

Figure 3. TGA profiles of CBC-800, CBC/PANI-T-0.1 and CBC/PANI-P-0.1 composites under N_2 flow at a temperature ramp of 20°C/min.

In the CBC-800 sample, there was no obvious weight loss before 700°C, indicating that after pyrolysis, the CBC-800 sample without any other impurities was completely carbonized. In the TGA curves of CBC/PANI-T-0.1 and CBC/PANI-P-0.1 composites, both show weight loss before 150°C, which was caused by the volatilization of water molecules in the samples when the samples are placed in air environment[33]. Due to the different kinds of doping acids, the thermal stabilities of the synthesized CBC/PANI composites were also different. The CBC/PANI-P-0.1 sample experienced a large amount of weight loss in the temperature range of 220~600°C, which was mainly caused by the oxidation and decomposition of the PANI polymer, and the weight loss rate was approximately 20 wt%was[34]. Additionally, the CBC/PANI-T-0.1 composite showed more weight loss of approximately 40 wt% in the temperature range between 285 and 600°C, which was mainly caused by the decomposition of p-benzenesulfonic acid ions and the oxidation and decomposition of polyaniline molecules. It can be observed from the TGA diagrams of the CBC/PANI composites that in the decomposition stage of 200~600°C, the initial decomposition temperature of the CBC/PANI-T-0.1 sample was higher, suggesting that the thermal stability of the CBC/PANI-T-0.1 composite prepared by organic acid is better than those of other samples. According to the analysis of thermal weight loss, the weight loss rate of CBC/PANI-T-0.1 was higher than those of other samples, which indicates that there are more PANI molecules coated on the CBC surface in the CBC/PANI-T-0.1 composite.

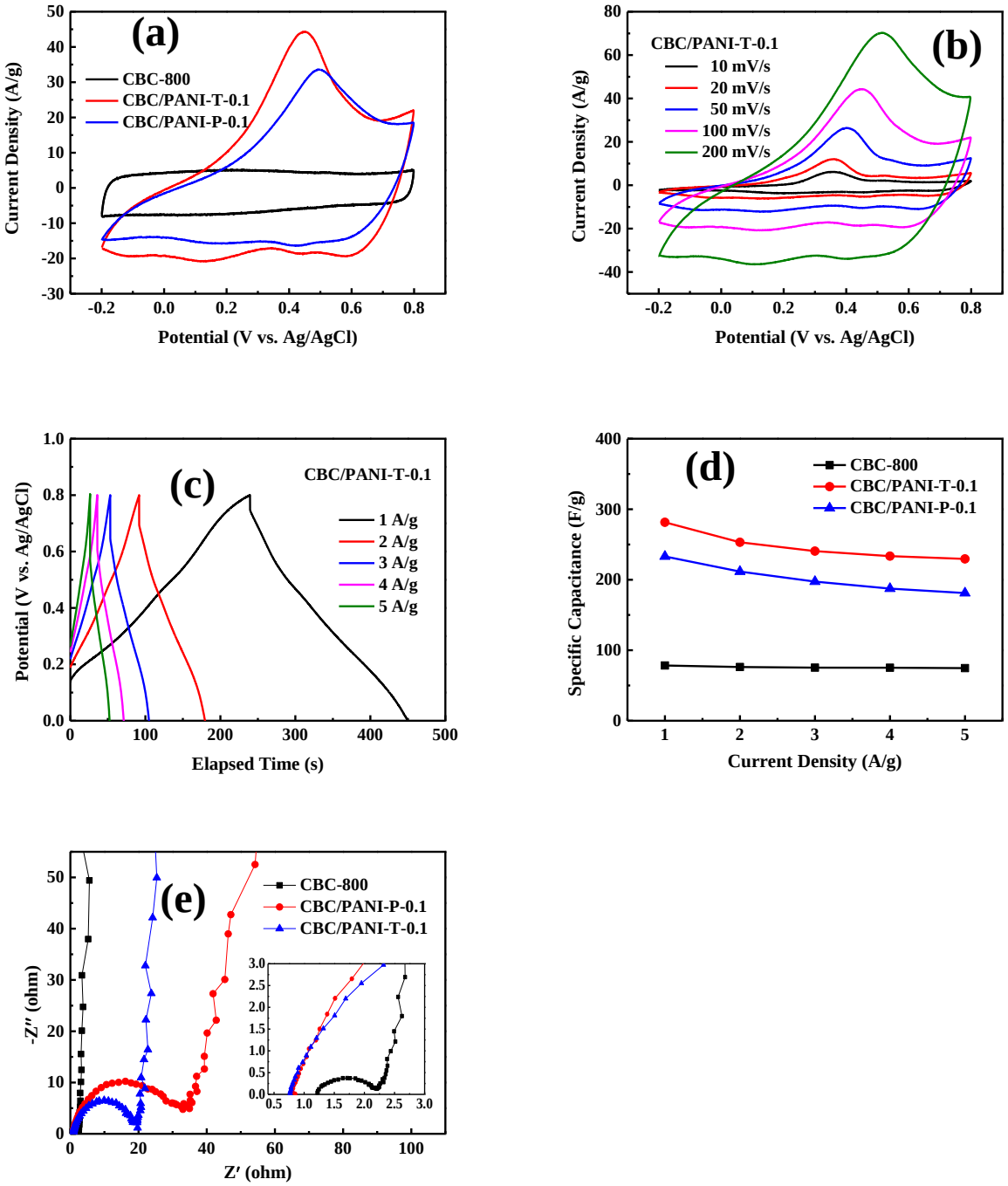

Figure 4. (a) CV curves of the CBC-800, CBC/PANI-T-0.1 and CBC/PANI-P-0.1 composites at a scan rate of 100 mV/s; (b) CV curves of the CBC/PANI-T-0.1 composite at various scan rates; (c) GCD curves at various current densities for the CBC/PANI-T-0.1 composite; (d) specific capacitance of the CBC-800, CBC/PANI-T-0.1 and CBC/PANI-P-0.1 composites at various current densities; (e) Nyquist plots of the CBC-800, CBC/PANI-T-0.1 and CBC/PANI-P-0.1 composite electrode materials.

The capacitance performance of CBC/PANI composites was tested with CV and GCD. The CV curve of the CBC-800 electrode measured at -0.2-0.8 V is shown in Figure 4 and shows an approximately rectangular shape, indicating favourable electric double-layer capacitance characteristics[35]. For

CBC/PANI composites, the CV curve shape does not show an ideal rectangular shape of carbon electrode materials, but there is a broad peak, demonstrating that the capacitance can be attributed to the double-layer capacitance of CBC and the faradic pseudo-capacitance of PANI[34]. In Figure 4a, it can be noted that the CV curve area of CBC/PANI-T-0.1 is larger than that of CBC-800 and CBC/PANI-P-0.1 at the same scan rate, illustrating that the CBC/PANI-T-0.1 electrode possesses a higher specific capacitance. Compared with CBC-800 nanofibres derived from bacterial cellulose, the CBC/PANI composite exhibits greater capacitive performance because the double layer of CBC contains more active sites and the Faraday redox reaction occurs in the presence of PANI[36].

Among various CBC/PANI composite electrodes, the CBC/PANI-T-0.1 electrode exhibits superior capacitive characteristics, which is facilitated by the successful synthesis of PANI to provide rapid redox reactions, and the CBC three-dimensional network structure promotes rapid ion transport. Irregular cyclic voltammetry curves of the CBC/PANI-T-0.1 composite electrode (at 10, 20, 50, 100, and 200 mV/s) are displayed in Figure 4b. It can be clearly seen from Figure 4b that a larger scanning rate results in a larger integral area of the CV curve while maintaining the redox peak of the PANI, demonstrating the superior rate characteristics of the material.

The GCD curves of the CBC/PANI-T composite at 1~5 A/g are depicted in Figure 4c, displaying quasi-triangular shapes with a few deformations due to Faradic pseudo-capacitance based on the redox reaction of PANI during the charge-discharge process. In addition, the volume of the PANI polymer will increase and decrease during this process, which may lead to an increase in internal resistance. This is the reason for the voltage drop during discharge. As depicted in Figure 4d, compared to the three electrode materials, CBC/PANI-T-0.1 showed the best capacitive behaviour; CBC/PANI-T-0.1, CBC-800 and CBC/PANI-P-0.1 at 1A/g current density, had specific capacitances of 281.5 F/g, 78.3 F/g and 233F/g, respectively. In addition, comparing the capacitance behaviour of the CBC/PANI polymer in the cycle test, it was found that the CBC/PANI-T-0.1 electrode material retained 81.5% of the initial capacitance and that the CBC/PANI-P-0.1 electrode material retained only 77.7% at the high discharge current density of 5 A/g, most likely resulting from the 3D network structure of CBC nanofibres and the greater amount of PANI coating on the surface of CBC nanofibres, which can be beneficial for ion fast diffusion and transport, providing more active sites and Faradic pseudo-capacitance. Figure 4(e) shows Nyquist curves of different samples (CBC-800, CBC/PANI-T-0.1 and CBC/PANI-P-0.1) at 100 kHz to 0.01 Hz. The curves of the three samples are very similar, and the Nyquist points on the impedance spectrum have a clear frequency change. In the low-frequency region, the impedance spectrum shows a straight line, and the impedance of the high-frequency region exhibits a good semicircular curve. The value of R_s (the axial intercept represents the bulk resistance) for CBC-800 was measured to be approximately 1.22 Ω. However, the values of R_s for CBC/PANI-T-0.1 and CBC/PANI-P-0.1 are only 10.77 and 0.85 Ω, consistent with lower bulk resistance. The results of this analysis proved that the presence of PANI can enhance the electrical conductivity of the CBC sample. In addition, the semicircular diameter of the CBC/PANI-P-0.1 sample is larger than that of CBC/PANI-T-0.1, indicating that the charge transfer resistance of the CBC/PANI-T-0.1 sample is lower. At low frequencies, the larger the slope of the line is, the smaller the diffusion impedance is, and the better the capacitance performance is[37]. For the two composites, the oblique line of the sample CBC/PANI-T-0.1 is more inclined to the

Y axis, its slope is much larger, and the diffusion impedance of this sample is smaller. In other words, the CBC/PANI-T-0.1 sample exhibits much better capacitance performance.

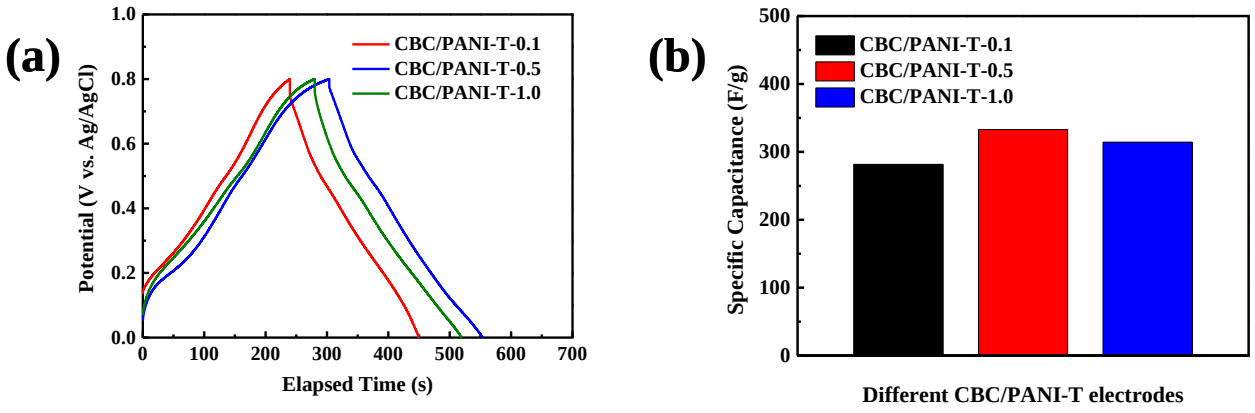

FFigure 5. (a) GCD curves of the different CBC/PANI-T electrodes measured using a three-electrode cell in a 1 M H_2SO_4 aqueous electrolyte at a current density of 1 A/g; (b) specific capacitance values of different CBC/PANI-T electrodes at 1 A/g.

As shown in Figure 5a, the CBC/PANI-T-0.5 sample had the longest discharge time, suggesting that it possesses the highest specific capacitance. Increasing the concentration of the TsOH aqueous solution from 0.1 to 0.5 M led to an increase in the specific capacitance (at 1.0 A/g) from 281.5 to 324.8 F/g (Figure 5b), owing to the increasing amounts of PANI coated on the CBC nanofibres. The introduction of conductive PANI into the CBC nanofibre enhanced the conductivity, reduced the internet resistance and contributed a large pseudocapacitance due to the oxidation-reduction reaction. However, when the concentration of the TsOH aqueous solution increased to 1.0 M, the microstructure (Figure S1) of the as-prepared CBC/PANI-T-1.0 sample became agglomerated due to the faster polymerization rate of the highly concentrated TsOH aqueous solution, which resulted in a lower specific capacitance (314.2 F/g). In short, the CBC/PANI-T-0.5 electrode exhibited the best capacitive performance. Table 2 shows the comparison of the specific capacitance of the published polyaniline and carbon material electrodes and this study. It is clear that the specific capacitance of CBC/PANI-T-0.5 prepared in this study is similar or higher than those reported in other papers.

Table 1. Comparison of the specific capacitance values of carbon/PANI materials reported in this and other works.

Material	Electrolyte	Current density	specific capacitance ($F\ g^{-1}$)	References
CBC-KOH	6 M KOH	0.1 A g^{-1}	241.8	[38]
SDG/PANI (1:1)	1 M H_2SO_4	10 A g^{-1}	320	[34]
KPC/PANI	1 M H_2SO_4	1.3 A g^{-1}	136	[33]

Material	Electrolyte	Current density	specific capacitance ($F\ g^{-1}$)	References
GH/SWCNTs/PANI	1 M H_2SO_4	0.5 A g^{-1}	145.4	[39]
MCF/N-CS/PANI	1 M NaCl	1 mA cm^{-2}	139.6	[40]
CNF/PANI	1 M H_2SO_4	1 A g^{-1}	234	[41]
LC/PAIN	6 M KOH	1A g^{-1}	336	[42]
AC/PANI	1 M H_2SO_4	1.5 mA cm^{-2}	228	[43]
CBC/PANI	1 M H_2SO_4	1A g^{-1}	324.8	This work

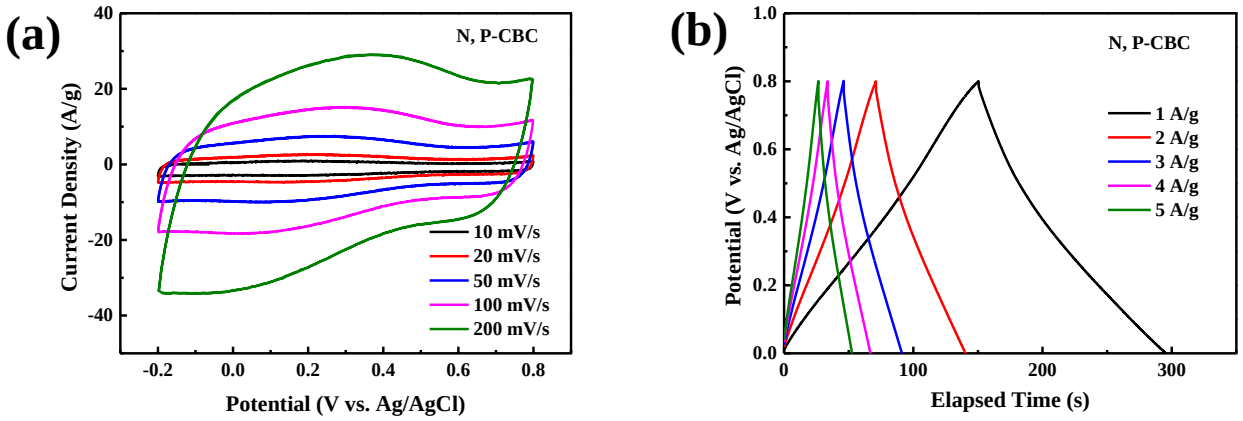

Figure 6. CV curves (a) and GCD curves (b) of N, P-CBC electrode in 1 M H_2SO_4

To further explore the practical application of the CBC/PANI-T-0.5 electrode in supercapacitor devices, the CBC/PANI-T-0.5 electrode material synthesized herein as a cathode and previously reported N,P-CBC[29] as an anode material were co-assembled into an asymmetric supercapacitor (ASC). N,P-CBC exhibited excellent specific capacitance of 184.6 F/g at 1A/g performance, as shown in Figure 6. According to the calculation of specific capacitance under the same conditions (voltage window, current density), the optimal active material mass ratio of the assembled asymmetric supercapacitor was m[CBC/PANI-T-0.5] : m[N, P-CBC]=0.57 : 1. Then, the electrochemical properties were tested as follows.

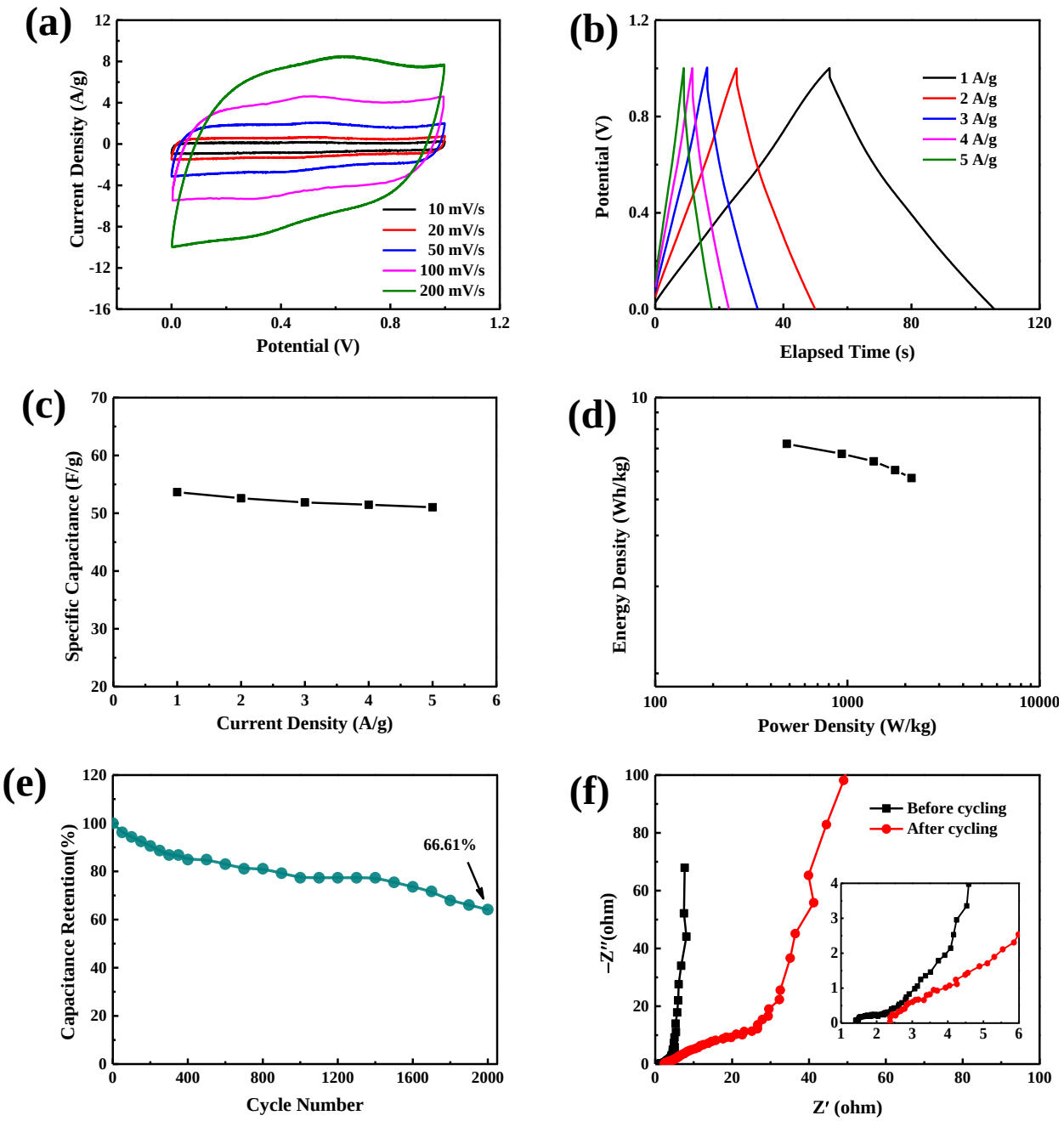

Figure 7. (a) CV curves of CBC/PANI-T-0.5//N, P-CBC asymmetric supercapacitor device at various scan rates in 1 M H_2SO_4; (b) GCD curves of the asymmetric supercapacitor at 1~5 A/g; (c) curve of specific capacitance values vs current density of the asymmetric supercapacitor; (d) Ragone curves for the asymmetric supercapacitor; (e) cycling performance of the CBC/PANI-T-0.5//N,P-CBC asymmetric supercapacitor in 1 M H_2SO_4 at 5 A/g; and (f) EIS plot of the asymmetric supercapacitor.

The as-fabricated CBC/PANI-T-0.5//N,P-CBC asymmetric supercapacitor demonstrates a typical capacitive behaviour under a voltage range of 0~1.0 V in 1 M H_2SO_4, as depicted by the CV and GCD curves given in Figure 7a and 7b, respectively. Figure 7a shows that the CV curve of the ASC has an irregular rectangular shape, which occurs because the CBC provides both an electric double layer capacitance and faradaic capacitance based on PANI. The shape of the CV retains the original shape

when the scanning rate is increased, implying predominant rate performance and capacitive performance for the ASC device. Moreover, it can be observed that the GCD curves (Figure 7b) are an approximate isosceles triangle, which also confirms the ideal reversible capacitive characteristic. Figure 7c shows the specific capacitance of the CBC/PANI-T-0.5//N,P-CBC ASC at a current density of 1 to 5 A/g in a 1 M H_2SO_4 aqueous solution; the capacitance value was 53.7 F/g at a current density of 1 A/g and maintained 95.1% capacitance (51 F/g), when the current density increased to 5 A/g. The obtained Ragone plot is given in Figure 7d. The CBC/PANI-T-0.5//N,P-CBC ASC device energy density achieved 6.92 Wh/kg at a power density of 483.7 W/kg. The energy density and power density of chestnut shell/PANI-prepared supercapacitors are 15.4 Wh/kg and 252 W/kg[44]. The CBC/PANI-T-0.5//N,P-CBC ASCs had good cycle stability and retained 66.61% of their initial capacitance at 5 A/g after 2000 cycles (Figure 7e). As shown in Figure 7f, the internal resistance of the device increased after cycling charge and discharge due to expansion and contraction of the PANI skeleton, resulting in a decrease in the specific capacity for the CBC/PANI-T-0.5//N,P-CBC ASC device.

4. CONCLUSIONS

In summary, nanofibre-like CBC/PANI composites have been successfully synthesized via in situ polymerization with different dopant acids (i.e., H_3PO_4 and TsOH). The obtained CBC/PANI-T-0.5 composite exhibited a much higher specific capacitance than the CBC-800 nanofibres and CBC/PANI-P-0.1 composite. The specific capacitance of CBC/PANI-T-0.5 reached 324.8 F/g at a current density of 1 A/g. The CBC/PANI-T-0.5 composite with excellent electrochemical characteristics due to the 3D nanofibre network structure of CBC nanofibres and the synergistic effect of CBC and PANI together resulted in a high capacitance effect. The introduction of conductive PANI into the CBC nanofibres enhanced the conductivity and contributed a large pseudo-capacitance due to the oxidation-reduction reaction. The as-assembled CBC/PANI-T-0.5//N,P-CBC asymmetric supercapacitor showed good capacitance, great rate performance and good long-term cycling performance. These results distinctly demonstrate that the CBC/PANI-T composite is an effective electrode material candidate in the application of energy storage devices.

ACKNOWLEDGEMENTS

This work was supported by the Scientific Cultivation and Innovation Fund Project of Jinan University (nos. 21617427 and 21617422) and the Guangdong Science and Technology Project Fund (no. 2015A030310488).

SUPPORTING INFORMATION

Equations:

The specific capacitance value of these electrodes was calculated by the following equation:

$$C = \frac{I \times \Delta t}{m \times V} \quad (1)$$

where *C* is the specific capacitance (F/g), *I*/*m* is the current density (A/g), Δ*t* is the discharge time (s), and *V* is the potential (V).

Electrochemical Measurements of the Asymmetric Supercapacitors: The asymmetric supercapacitor (ASC) was fabricated by using CBC/PANI-T composite as the positive electrode material and N,P-CBC nanofibre as the negative electrode material. The mass ratio of CBC/PANI-T composite to N,P-CBC nanofibre was determined to be 0.57 using the following equation (2): where m is the loading mass of the electrode (g), C is the specific capacitance (F/g), and V is the potential (V).

$$\frac{m_+}{m_-} = \frac{C_- \times V_-}{C_+ \times V_+} \quad (2)$$

The energy density and power density of the asymmetric supercapacitor according to equations (3) and (4):

$$E = \frac{C \times \Delta U^2}{7.2} \quad (3)$$

$$P = \frac{E}{\Delta t} \quad (4)$$

where E is the energy density (Wh/kg), C is the specific capacitance (F/g), ΔU is the potential (V), P is the power density (W/kg), and Δt is the discharge time (s).

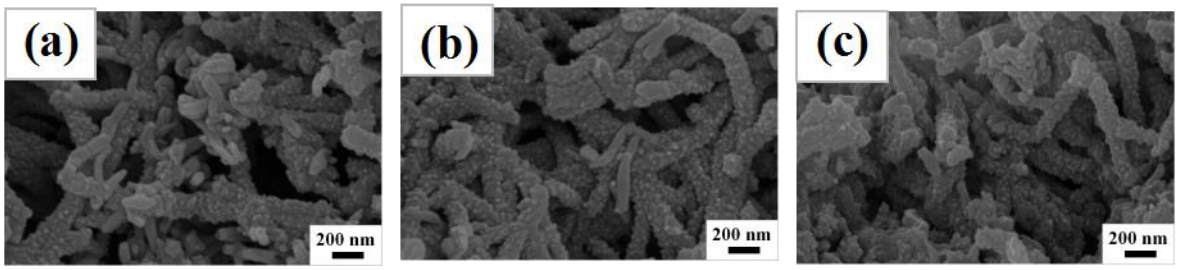

Figure S1 SEM image of CBC/PANI-T composites prepared by various concentrations of TsOH aqueous solution (a) 0.1 M; (b) 0.5 M; (c) 1.0 M

References

1. P. Simon, Y. Gogotsi and B. Dunn, *Mater. Sci.*, 343 (2014) 1210.
2. Poonam, K. Sharma, A. Arora and S. K. Tripathi, *J. Energy Storage* , 21 (2019) 801.
3. Y. G. Wang, Y. F. Song and Y. Y. Xia, *Chem.Soc.Rev.*, 45 (2016) 5925.
4. M. R. Lukatskaya, B. Dunn and Y. Gogotsi, *Nat. Commun.,* 7 (2016) 12647.
5. Z. Q. Li, M. W. Tian, X. T. Sun, H. T. Zhao, S. Z. Zhu and X. S. Zhang, *J. Alloys Compd.,* 782 (2019) 986.
6. F. Q. Jin, H. Tong, L. Lu, Q. Meng, S. H. Yue, B. Ding and X. G. Zhang, *J. Alloys Compd.,* 787 (2019) 36.
7. M. Serrapede, A. Rafique, M. Fontana, A. Zine, P. Rivolo, S. Bianco, L. Chetibi, E. Tresso and A. Lamberti, *Carbon*, 144 (2019) 91.
8. Y. J. Kang, H. Chung, M. S. Kim and W. Kim, *Appl. Surf. Sci.*, 355 (2015) 160.
9. S. P. Xi, Y. R. Kang, S. X. Qu and S. S. Han, *Mater. Lett*., 175 (2016) 126.

10. R. Z. Zhang, J. J. Ding, C. Liu and E. H. Yang, *ACS Appl. Energy Mater.*, 1 (2018) 2048.
11. X. J. He, R. C. Li, J. S. Qiu, K. Xie, P. H. Ling, M. X. Yu, X. Y. Zhang and M. D. Zheng, *Carbon*, 50 (2012) 4911.
12. T. X. Shang and X. J. Jin, *J Solid State Electrochem*, 20 (2016) 2029.
13. S. K. Hussain, B. Dudem and J. S. Yu, *Appl. Surf. Sci*., 478 (2019) 846.
14. X. C. Chen, X. S. Zhu, Y. H. Xiao and X. D. Yang, *J. Electroanalytical Chem.*, 743 (2015) 99.
15. S. Liu, L. Yao, Y. Lu, X. L. Hua, J. Q. Liu, Z. Yang, H. Wei and Y. Y. Mai, *Mater. Lett.*, 236 (2019) 354.
16. S. T. Li, Y. N. Duan, Y. Teng, N. Fan and Y. Q. Huo, *Appl. Surf. Sci.*, 478 (2019) 247.
17. Q. S. Wang, Y. F. Zhang, H. M. Jiang, X. J. Li, Y. Cheng and C. G. Meng, *Chem. Eng. J.*, 362 (2019) 818.
18. F. Yu, X. Xiong, L. Y. Zhou, J. L. Li, J. Y. Liang, S. Q. Hu, W. T. Lu, B. Li and H. C. Zhou, *J. Mater. Chem. A,* 7 (2019) 2875.
19. M. Zhang, Y. T. Li and Z. R. Shen, *J. Power Sources,* 414 (2019) 479.
20. Y. Huang, C. L. Zhu, J. Z. Yang, Y. Nie, C. T. Chen and D. P. Sun, *Cellulose,* 21 (2013) 1.
21. Z. M. Zhao, Y. J. Hua, C. H. You, Y. Li, Liu H, H. H. Huang, X. F. Wu, Y. Z. Wang and C. T. Wang, *Mater. Res. Innov*, 21 (2016) 91.
22. E. Jazaeri and T. Tsuzuki, *Cellulose,* 20 (2013) 707.
23. A. Eftekhari, L. Li and Y. Yang, *J. Power Sources*, 347 (2017) 86.
24. X. X. Wang, M. Xu, Y. L. Fu, S. Y. Wang, T. Yang and K. Jiao, *Electrochim. Acta*, 222 (2016) 701.
25. Y. Yuan, W. L. Zhu, G. Du, D. Z. Wang, J. L. Zhu, X. H. Zhu and G. Pezzotti, *Electrochim. Acta*, 282 (2018) 286.
26. M. A. Bavio, G. G. Acosta and T. Kessler, *J. Power Sources,* 245 (2014) 475.
27. Q. Cheng, J. Tang, N. Shinya and L.C. Qin, *J. Power Sources*, 241(2013) 423.
28. S. K. Simotwo and V. Kalra, *Electrochim Acta,* 268 (2018) 131.
29. D. B. Kong , L. Cao , Z. M. Fang , F. L. Lai , Z. D. Lin , P. Zhang and W. Li , *Ionics,* (2019) 1.
30. J. Li, K. Fang, Q. Hong, S. P. Li and W. M. Mao, *Synth. Met.*, 142 (2004) 107.
31. X. R. Fan , X. D. Yan , Y. H. Yu , J. L. Lan and X. P. Yang, *Electrochim Acta*, 216 (2016) 355.
32. Q. Wang , J. Yan , Z. J. Fan , T. Wei , M. L. Zhang and X. Y. Jing , *J. Power Sources*, 247 (2014) 197.
33. D. Y. Lei, K. H. Song, X. D. Li, H. Y. Kim, B. S. Kim, *J. Mater. Sci*., 52 (2017) 2158.
34. J. J.Yao, P. Ji, N. Sheng, F. Y. Guan, M. H. Zhang, B. X. Wang, S. Y. Chen and H. P. Wang, *Electrochim Acta*, 283 (2018) 1578.
35. R. Gupta, N. Vadodariya, A. Mahto, J. P. Chaudhary, D. B. Parmar, D. N. Srivastava, S. K. Nataraj and R. Meena, *J. Appl.Electrochem.*, 48 (2018) 37.
36. J. H. Liu, X. Y. Xu, W. B. Lu, X. B. Xiong, X. O. yang, C. H. Zhao, F. Wang, S. Y. Qin, J. L. Hong, J. N. Tang and D. Z. Chen, *Electrochim Acta*, 283 (2018) 366.
37. H. Wu, Y. N. Zhang, W. Y. Yuan, Y. X. Zhao, S. H. Luo, X. W. Yuan, L. X. Zheng and Laifei Cheng, *J. Mater. Chem. A*, 6 (2018) 16617.
38. X. J. Wang, D. B. Kong, B. Wang, Y. Song and Linjie Zhi, *Sci. China Chem*., 9 (2016) 713.
39. X. X. Du, F. B. Luo, Y. Y. Guo, Q. Q. Zhu, F. Xiao, K. Wu and Mangeng Lu，*J.Appl. Polym. Sci*，136 (2019) 46948.
40. Q. Z. Liu, Z. H. Chen, S. S. Jing, H. Zhuo, Y. J. Hu, J. C. Liu, L. X. Zhong, X. W. Peng and C. F. Liu, *J. Mater. Chem. A*, 6 (2018) 20338.
41. M. Yanilmaza, M. Diricana, A. M. Asiric and X. W Zhang, *J. Energy Storage*, 24 (2019) 10766.
42. K. L. Wang, Y. H. Cao, X. M. Wang, M. AndreaCastro, B. Luo, Z. R. Gu, J. Liu, J. D. Hoefelmeyer and Q. H. Fan, *J. Power Sources*,307 (2016) 462.
43. I. I. G. Inal, Y. Gokce and Z. Aktas, Waste tea derived activated carbon/polyanilinecomposites as supercapacitor electrodes , 2016 IEEE International Conference on Renewable Energy Research and Applications (ICRERA)，Birminghan， UK, 2016, 458-462.

44. H. P. Wang, G. F. Ma,Y. C. Tong and Z. R. Yang, *Ionics,* 24 (2018) 3123.